INTERNATIONAL JOURNAL OF CLIMATOLOGY
Int. J. Climatol. **35**: 2164–2179 (2015)
Published online 11 August 2014 in Wiley Online Library
(wileyonlinelibrary.com) DOI: 10.1002/joc.4120

RMetS
Royal Meteorological Society

Characterization of the 1970s climate shift in South America

Martín Jacques-Coper[a]* and René D. Garreaud[b]
[a] *Oeschger Centre for Climate Change Research and Institute of Geography, University of Bern, Switzerland*
[b] *Departamento de Geofísica, Universidad de Chile, Santiago, Chile*

ABSTRACT: The 1976–1977 cold-to-warm sea surface temperature (SST) shift in the tropical Pacific Ocean, which has been associated with a phase change of the Pacific Decadal Oscillation (PDO) index, separated a 'La Niña-like' decadal regime from an 'El Niño-like' one. In this article, we analyse the differences of mean of annual and austral-summer (DJF) temperature, precipitation, and sea-level pressure (SLP) over South America (SA) between 1961–1973 and 1978–1990, and explore the occurrence of significant shifts in their time series. Our sources are instrumental records, gridded interpolated data, and reanalyses. Although major regional differences in the intensity of the signal are detected, the climate shift is identified in all variables. In the mid-1970s at annual level, reanalysis SLP data reveal the onset of a step-like anticyclonic circulation anomaly in the southern tip of SA and an abrupt weakening of the Southeast Pacific Subtropical Anticyclone (SEPA). This latter feature may have partly induced the rapid warming observed along the tropical–extratropical west coast of the continent through the weakening of the cold Humboldt current system. An abrupt warming was also detected in surface air temperature (SAT) composites located along the coast of the northern part of SA and in Southeastern SA (SESA). During summer, we found a particularly conspicuous shift-like warming over Southern South America (SSA, comprising Patagonia). Besides, a shift-like increase (decrease) in annual mean precipitation is observed over Central Argentina and in the tropics, to the south (north) of 10°S. In line with previous studies, we conclude that both the interannual (El Niño-Southern Oscillation, ENSO) and the interdecadal (PDO) variability modes seem to have had an incidence in the manifestation of the 1970s climate shift, and that its magnitude appears to be unprecedented during the 20th century, as shown in particular by century-long SAT composites from northern Chile and SSA.

KEY WORDS climate shift; 1970s; South America; PDO; South Pacific; Patagonia; warming

Received 27 January 2014; Revised 4 June 2014; Accepted 6 July 2014

1. Introduction

The temporal variability of the climate system comprises cycles from a wide range of frequencies and also stepwise changes between different states, called *climate shifts* (Miller *et al.*, 1994). To be considered as such, a certain transition has to occur during a period considerably shorter than the characteristic permanence of the corresponding states (Minobe, 1997). Such a climate shift was reported in the North Pacific between 1976 and 1977 and becomes apparent in the time series of the Pacific Decadal Oscillation (PDO), the principal source of climate variability in the North Pacific during the 20th century (Mantua and Hare, 2002). The PDO index can be modelled as a shift sequence that accounts for the major part of the series' total variance (Mantua *et al.*, 1997). The years 1925, 1947 and 1977 correspond to polarity changes between stable periods of that index. The last one defines a cold-to-warm transition in the tropical Pacific within 1 year (Giese *et al.*, 2002). This event had now well-known effects, such as the intensification of the Aleutian Low in the Northeast Pacific, which was more pronounced during boreal winter (Trenberth, 1990), and changes in the ocean circulation (Deser *et al.*, 1996; Zhang *et al.*, 1998; Chao *et al.*, 2000), which affected the atmosphere and the ecosystems in the whole Pacific Basin (Chavez *et al.*, 2003).

The origin of the 1970s event remains uncertain. It has not been established whether it corresponds to a unique phenomenon or rather to a rapid phase transition linked to a cyclic mode. In association with this shift, some studies suggest teleconnection mechanisms induced by tropical sea surface temperature (SST) forcing (Trenberth, 1990; Graham, 1994; Miller *et al.*, 1994). These mechanisms can also be observed in model experiments (Huang *et al.*, 2005). The resemblance between the spatial patterns of SST variability at interannual and longer time scales is stressed by Tanimoto *et al.* (1993) and Mantua *et al.* (1997). In this sense, Zhang *et al.* (1997) state that the interdecadal variability fields of SST, sea-level pressure (SLP) and wind stress over the Pacific exhibit similar spatial patterns as those of the El Niño-Southern Oscillation (ENSO) interannual variability. Therefore, the 1976–1977 transition has been described as separating a 'La Niña-like' interdecadal regime from an 'El Niño-like' one (Garreaud and Battisti, 1999). However, while the PDO pattern is more pronounced in the extratropics and less pronounced in the tropics, the opposite is valid for ENSO (Mantua and Hare, 2002). Furthermore, it is not

* Correspondence to: M. Jacques-Coper, Oeschger Centre for Climate Change Research and Institute of Geography, University of Bern, Hallerstrasse 12, CH-3012 Bern, Switzerland. E-mail: jacques@giub.unibe.ch

clear yet whether a slow oscillation modulates the frequency of ENSO extreme events or if these latter ones trigger the regime shifts (Yasunaka and Hanawa, 2005).

Various possible causes have been suggested for the origin of the SST anomalies related to the climate shift. For instance, Giese *et al.* (2002) state that the SST perturbations originated in the Southern Hemisphere, whereas Montecinos *et al.* (2007) explain the interdecadal changes in thermocline and SST in the eastern equatorial Pacific and along the western coast of South America (SA) through zonal wind anomalies in the western equatorial Pacific.

In addition, it is also not clear if an event like the 1976–1977 climate shift in the North Pacific could have been linked to anthropogenic global warming (Trenberth, 1990; Kerr, 1992). Meehl *et al.* (2009) interpret the shift as a consequence of changes in external forcing, particularly the increase in atmospheric greenhouse gases, superimposed upon inherent decadal fluctuations of the Pacific climate system.

While most of the previous research on this topic has focused on the effects of the climate shift in the Northern Hemisphere (e.g. Minobe, 1997; Hartmann and Wendler, 2005; Litzow, 2006), very few studies have dealt with its effects in the Southern Hemisphere. Agosta and Compagnucci (2008) analysed the austral summer circulation transition of 1976–1977 in Southern South America (SSA) based on the NCEP/NCAR reanalysis I (NNR). Among their main findings related to the climate state in SSA after the shift are: (1) a reduced midlatitude cyclonic activity, leading to less dry events over Central Western Argentina (CWA), and (2) the expansion of the Subtropical Atlantic Anticyclone over the continent at tropical and subtropical latitudes, inducing a more northerly flow and moisture advection into CWA. They concluded that this event seems to be rather unique in the 20th century and not solely related to the PDO variability. Other papers, although not necessarily focused on this transition, found changes in SAT and precipitation (mean values and trends) over SA around 1976–1977. For instance, Collins *et al.* (2009) analysed the SAT difference between 1948–1975 and 1976–2007 based on NNR, identified a marked SAT increase over SA around mid-1970s (especially for DJF over SSA), stressed the good agreement of subcontinental SAT time series with the PDO index, and stated that ENSO cannot be largely responsible for the observed temperature differences. However, they did not bring this observation into a continental context among other variables, nor offered a possible dynamical explanation for it. Liebmann *et al.* (2004) found that the positive January-to-March precipitation trend during 1976–1999 over southern Brazil (23°–29°S; 47°–53°W) was twice as large as during 1948–1975 and explained it through an increased percentage of rainy days and larger amounts of precipitation per event. Marengo (2004) associated the mid-1940s and mid-1970s interdecadal precipitation regime changes over Amazonia with the varying frequency of El Niño events. In particular, the northern part of the basin showed wetter conditions between those transitions than after 1976, whereas the southern portion of the basin has exhibited a positive trend since early 1970s. A broader perspective into precipitation changes associated with the 1970s climate shift was provided by Carvalho *et al.* (2011), who studied the South American Monsoon System and documented a transition towards an earlier onset and a later demise of it around 1971–1972. This decadal modulation was related to the wetter period after the transition in the southern Amazon region and central Brazil. Consistently with these findings, sedimentological evidence from Laguna Mar Chiquita in SESA showed that an abrupt lake level increase took place in late 1970s, with the last quarter of the 20th century including the highest historically documented lake level in the last ∼240 years, pointing to a prominent wet period after the shift (Piovano *et al.*, 2002). Besides, other studies have analysed topics related to the 1970s shift along the west coast of SA, such as SAT trends (Falvey and Garreaud, 2009; Schulz *et al.*, 2012), the El Niño-like interdecadal variability of SST (Montecinos *et al.*, 2003) and the interdecadal variability of coastal upwelling along the arid coast of northern Chile and Peru (Vargas *et al.*, 2007).

Therefore, although previous work has described some specific aspects of the 1970s climate shift in SA, there is no systematic continental-scale characterization of its effects, which constitutes the novel contribution of this study. This article is structured as follows: Section 2 presents the data used in this work and the methodology employed to analyse the 1970s mean shift in the selected variables. Section 3 describes the results and explores in a broader temporal context two particular SAT composites. Discussions on the main results are included in Section 4, and Section 5 summarizes our findings.

2. Data and methodology

Our study area encompasses SA and the adjacent oceans. We analyse SAT, precipitation and SLP data from the Global Historical Climate Network instrumental database version 2 (GHCN, Peterson and Vose, 1997), as well as from the NNR (Kalnay *et al.*, 1996) and ECMWF ERA-40 (Uppala *et al.*, 2005) reanalysis products. Instrumental temperature data (annual means) from northern Chile were compiled by Schulz *et al.* (2012) from meteorological annals published by the Chilean Weather Service (DMC). We also analyse gridded SAT and precipitation fields from the University of Delaware datasets version 2.01 (UDel, Legates and Willmott, 1990a, 1990b), and SST from ERSSTv3b (Smith *et al.*, 2008) and HadISSTv1 (Rayner *et al.*, 2003). We are aware of possible biases in gridded data (especially interpolated precipitation data) due to the nonuniform geographic distribution of instrumental records in regions of high temporal variability and steep spatial gradients.

Our focus is on annual and austral-summer mean values, calculated as December-to-February (DJF) averages and assigned to the corresponding JF year. The selection criterion of instrumental SAT and SLP records corresponds

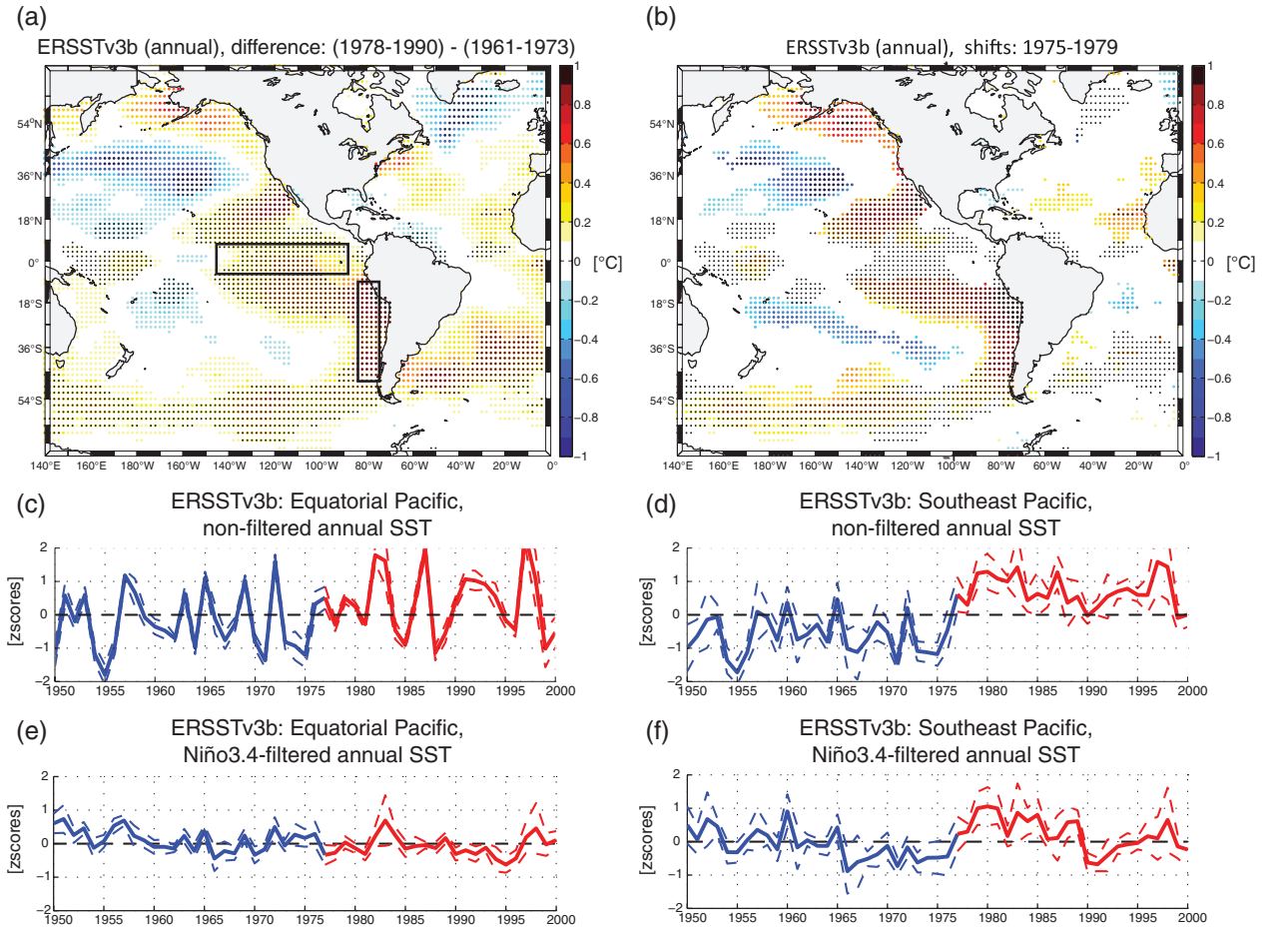

Figure 1. (a) Mean difference of annual SST (ERSSTv3b, °C) between 1961–1973 and 1978–1990. (b) Temperature shifts identified by Rodionov's test between 1975 and 1979, shown as differences between periods of 10 years before and 10 years after their detection. Blank zones do not show any significant shift. In both figures, statistically significant values (95%) of panel (a) are depicted by black dots; the corresponding gridpoints do not necessarily show a shift in their time series and therefore are not necessarily colour-filled in (b). (c–f) Time series of SST composite mean ± 1 SD, standardized with respect to 1961–1990 (zscores), corresponding to the areas enclosed in panel (a): (c) and (e) Equatorial Pacific (5°N–5°S; 90°–150°W) and (d) and (f) Southeast Pacific (10°–50°S; 75°–85°W). (c–d) Nonfiltered annual SST data and (e–f) Niño3.4-filtered annual SST data (see text).

to the availability of at least 80% of monthly data during 1961–1990. No gaps are filled for the calculation of means. To analyse the shift around mid-1970s, we first calculate the (1978–1990) – (1961–1973) difference of means of each variable. Then, by applying an ad hoc sequential Student's *t*-test (Rodionov, 2005), we identify statistically significant shifts that occurred between 1975 and 1979. For that, we consider a regime state persistence of at least 10 years and a significance level of 90% [parameter values of $L = 10$, $p = 0.1$ and $h = 1$, as specified in Rodionov (2005)]. According to these results, we form composites of standardized anomalies with respect to 1961–1990 to group the records from locations where similar manifestations of the shift are detected.

3. Results

3.1. Temperature

The difference of mean annual SST values between 1961–1973 and 1978–1990 (Figure 1(a)) shows the characteristic spatial pattern of the positive phase of the PDO in the Pacific Basin (Mantua *et al.*, 1997; Chen *et al.*, 2008): a symmetric warm anomaly around the equator and a polarity change between tropical (warm) and subtropical (cold) areas. In the Southern Hemisphere, this difference is statistically significant at 95% along the coast of Ecuador, Peru and Chile, and over the South Pacific around 60°S. Over the Atlantic Ocean, the most salient feature is the significant warming observed between 30° and 50°S. Although SST shifts are mostly detected at gridpoints where statistically significant mean differences are found (Figure 1(b)), especially along the southwestern coast of SA, no shifts are identified over the equatorial region. In contrast with these warming regions, the South Pacific Convergence Zone and a broad area around 35°N; 170°W exhibit abrupt cooling. The SST change pattern observed in ERSSTv3 is comparable to that obtained from the HadISSTv1 dataset (not shown), which also shows a symmetric tropical warming pattern in the eastern part of the Pacific Basin and cooling towards the subtropics in the western part of the basin. The SST warming at the western

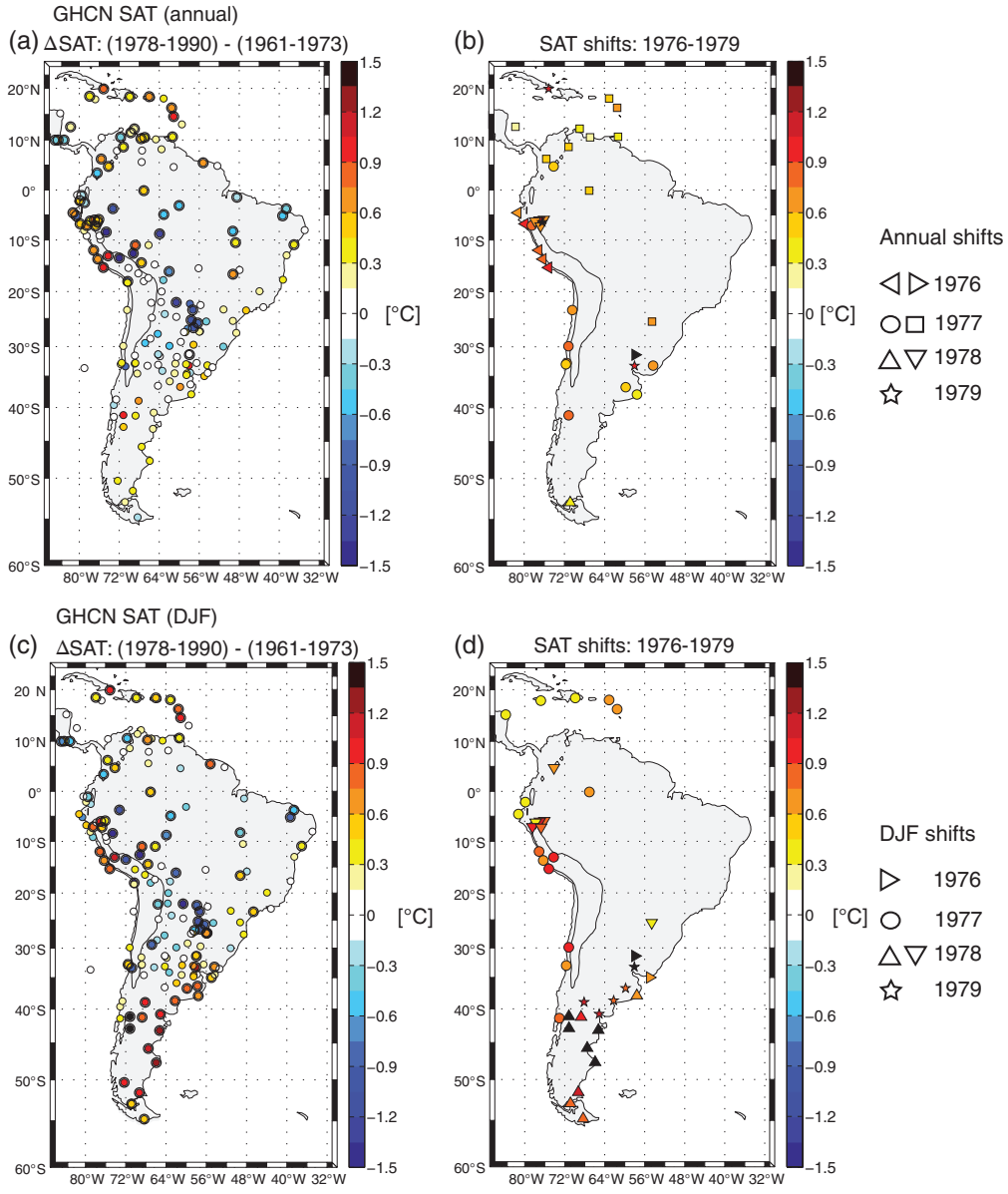

Figure 2. (a, c) Mean SAT (GHCN) difference (°C) between 1961–1973 and 1978–1990; statistically significant values (95%) are depicted by a thick marker edge. (b, d) SAT shifts identified by Rodionov's test between 1975 and 1979, shown as differences between periods of 10 years before and 10 years after their detection (see legends). Results are shown for (a, b) annual level and (c, d) austral summer (DJF) level. Different symbols for the same year denote different clusters, as shown in Tables 1 and 2 (see text for details). Over the continent, the solid contour depicts the 2000 m isoline.

coast of SA is clearly observed in both datasets. Nevertheless, HadISSTv1 shows a spatially more restricted warming pattern, in particular along the western coast of SA, and no significant warming in the equatorial Pacific. Consistently with these results, Deser *et al.* (2010) found for HadISSTv1 during the 20th century a subtler SST trend for the western coast of SA in comparison to ERSSTv3b and even cooling for the equatorial Pacific, a pattern which was described as an erroneous feature. Therefore, in the following analysis we will focus on ERSSTv3b.

Two regional composites have been selected to show their annual mean SST time series: Equatorial Pacific (5°N–5°S; 90°–150°W) and Southeast Pacific (10°–50°S; 75°–85°W). While the Equatorial region is characterized by a faintly positive SST trend of 0.12 °C decade^{-1} for the period 1950–2000 and no clear regime change is observed [ΔSST = 0.36 °C considering (1980–1990) – (1965–1975); Figure 1(c)], over the Southeast Pacific we observe slightly negative trends of −0.03 °C decade^{-1} for 1950–1975 and −0.09 °C decade^{-1} for 1978–2000, interrupted by a shift in 1976–1977 [ΔSST = 0.69 °C considering (1980–1990) – (1965–1975); Figure 1(d)]. This fact clearly shows that the positive SST trend of 0.17 °C decade^{-1}, observed over the Southeast Pacific during 1950–2000, does not properly describe its temporal SST variability.

Differences of annual mean SAT, calculated between 1961–1973 and 1978–1990 from 172 selected GHCN records (Figure 2(a)), show warming over the Caribbean,

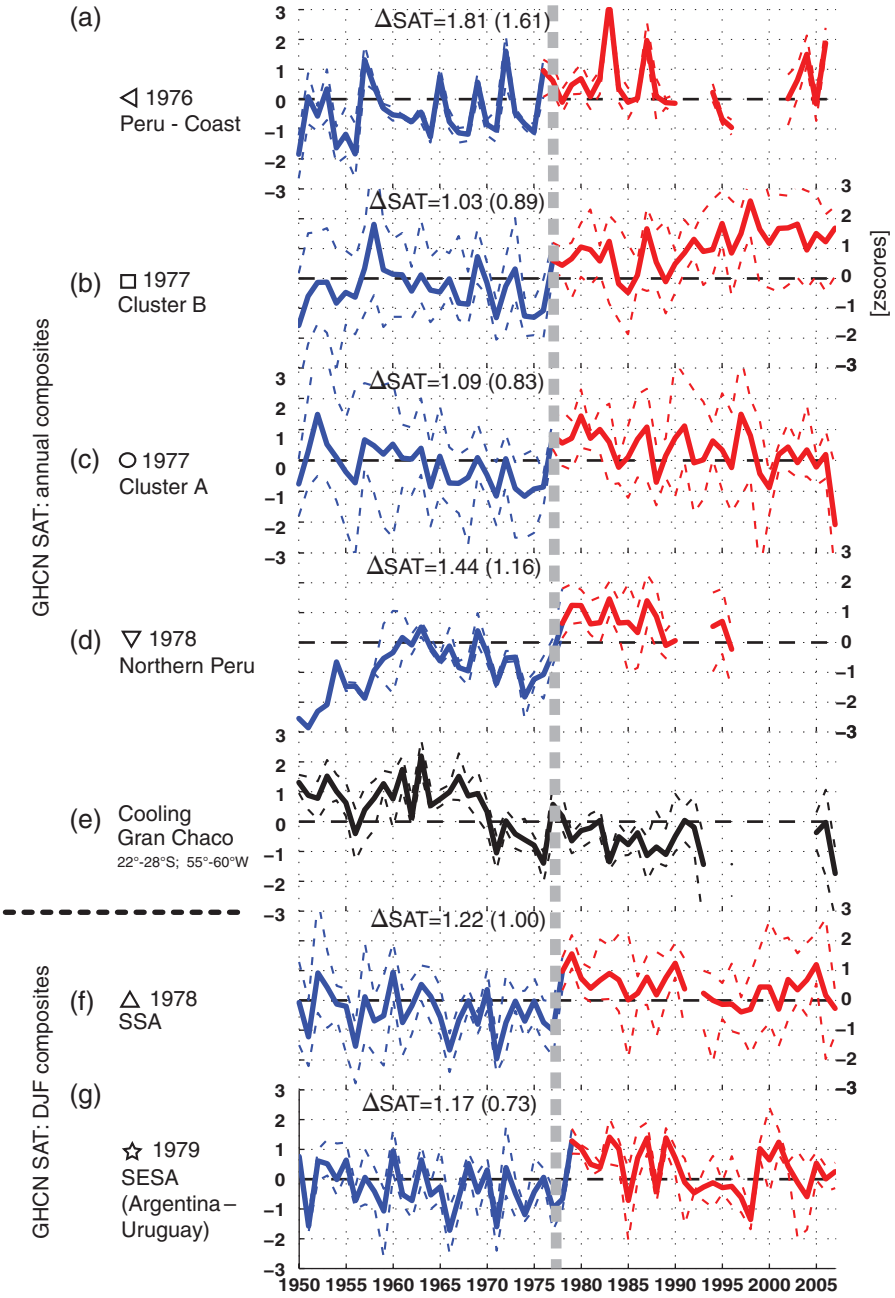

Figure 3. Composites of standardized anomalies of SAT records (GHCN) with respect to 1961–1990 (zscores), grouped according to the shift year detected by Rodionov's test (see Tables 1 and 2). (a–d) Composites of annual series showing a shift-like warming in (a) 1976, (b) 1977 (Cluster B), (c) 1977 (Cluster A), and (d) 1978; (e) Gran Chaco composite, associated with a region where cooling is observed and no shift is detected using Rodionov's test. (f–g) Composites of DJF series showing a shift-like warming in (f) 1978 and (g) 1979. Mean annual/DJF values are depicted by solid curves; dashed lines show the minimum and maximum value of the composite for each year. The vertical dashed line indicates the 1976/1977 transition. In each graphic, the legend at the upper left corner shows the (1980–1990) – (1965–1975) standardized SAT difference (ΔSAT) (zscores) resulting by considering (1) all years within those periods and (2) (in brackets) ENSO-neutral years only within those periods [i.e. ignoring El Niño (1966, 1973, 1977, 1983, 1987) and La Niña (1968, 1971, 1974, 1976, 1985, 1989) years].

Venezuela, Colombia, Ecuador, Peru, Chile, SSA (to the South of 35°S, including Patagonia), SESA (around the La Plata River in Argentina and Uruguay, 30°–40°S; 52°–60°W) and southeastern Brazil. This warming pattern contrasts with the cooling observed over the Amazon Basin and the Gran Chaco region (22°–28°S; 53°–61°W). The pattern of SAT change around the shift is also observed in the datasets of both reanalyses (not shown). Detected shifts are mostly found along the Pacific and Southwest Atlantic coasts (Figure 2(b)), a fact that suggests a direct influence on SAT of the observed increase in SST. Most of the shifts are detected in 1977, except for the Peruvian coast (1976), SESA (1977, 1978 and 1979), northern Peru (Amazonia and Sierra, 1978 and 1979) and the southern tip of SA (1978).

To visualize the temporal manifestation of the SAT shift, we form composites of standardized SAT anomalies with respect to 1961–1990. Records exhibiting a shift were

Table 1. Stations used to form the *annual* SAT composites (partly shown in Figures 3 and 6).

Shift year	Composite	GHCN station	Latitude (°N)	Longitude (°E)	Height (masl)
1976					
Figure 3(a)	Peru coast	Talara	−4.57	−81.25	90
		Chiclayo	−6.78	−79.83	34
		Lima-Callao/A	−12	−77.12	13
		Pisco	−13.75	−76.28	7
		San Juan	−15.38	−75.17	60
No Figure	Uruguay-Salto	Salto	−31.38	−57.95	33
1977					
Figure 3(c)	Cluster A	Bogotá/Eldora	4.72	−74.15	2548
		Cajamarca	−7.13	−78.47	2622
		Antofagasta	−23.43	−70.43	135
		La Serena	−29.9	−71.2	142
		Quintero	−32.78	−71.52	8
		Punta Ángeles	−33	−71.7	41
		Trenta y Tres	−33.22	−54.38	46
		Azul Aero	−36.75	−59.83	132
		Mar del Plata	−37.93	−57.58	21
		Bariloche Aer	−41.15	−71.17	840
Figure 3(b)	Cluster B	Juliana Airport	18.05	−63.12	9
		Le Raizet/Gua	16.27	−61.52	11
		San Andrés	12.58	−81.72	6
		Hato Airport	12.2	−68.97	67
		Piarco Int. A.	10.62	−61.35	15
		Caracas Cagigal	10.5	−66.9	1042
		Mérida	8.6	−71.18	1498
		Medellín/Olay	6.22	−75.6	1499
		Sao Gabriel D	−0.13	−67.08	90
		Juanjuí	−7.22	−76.72	363
		Puerto Stroessner	−25.53	−54.6	196
1978					
Figure 3(d)	Northern Peru	Yurimaguas	−5.90	−76.08	184
		Moyobamba	−6.03	−76.97	832
		Chachapoyas	−6.22	−77.83	2435
No Figure	Chile-Punta Arenas	Punta Arenas	−53	−70.85	37
Figure 3(e)	Gran Chaco (cooling)	Mariscal	−22.02	−60.6	181
		Puerto Casado	−22.28	−57.87	87
		Concepción	−23.42	−57.3	74
		Asunción Aero	−25.27	−57.63	101
		San Juan Bautista	−26.67	−57.15	126
		Pilar	−26.85	−58.32	56
		Encarnación	−27.32	−55.83	91
1977					
Figure 6(a)	Northern Chile	Arica	−18.33	−70.33	169
		Antofagasta	−23.43	−70.43	171
		Punta Tortuga	−29.90	−71.40	176

grouped according to (1) the year of occurrence of the shift and (2) the geographic distribution of the stations. Time series showing a shift in 1976, 1977 and 1978 were separated into two groups following their temporal evolution by means of cluster analysis with a minimum variance algorithm. Results are shown in Figure 3 and Table 1. For 1976, we find a cluster in the coast of Peru and also the station of Salto in Uruguay. For 1977, one cluster is mainly formed by stations from the southern half of SA (Cluster A), whereas the other one is constituted primarily by stations from the northern part of the continent and the Caribbean (Cluster B). In the case of 1978, one cluster groups stations from northern Peru and the other one corresponds to the station of Punta Arenas, in the southern tip of SA.

Nevertheless, there are also some regions which, although showing pronounced temperature differences around mid-1970s, do not exhibit any stepwise change in their time series. The Gran Chaco composite is presented as an example of those regions (Figure 3(e)). There, a negative SAT trend dominates during 1960–2000, hiding a slight warming in 1977.

At seasonal level, the temperature shift is especially striking during austral summer in instrumental data (Figure 2(c) and (d)). As for the annual case, we formed clusters for the years 1976, 1977 and 1978 (Table 2). In particular, a strong signal is found over SSA (>1.5 °C), as also observed in the reanalyses (not shown). Two DJF composites illustrate this aspect: eastern Patagonia (1978) and SESA (1979) (Figure 3(f) and (g)).

Table 2. Stations used to form the *austral summer* (*DJF*) SAT composites (partly shown in Figures 3 and 6).

Shift year	Composite	GHCN station	Latitude (°N)	Longitude (°E)	Height (masl)
DJF 1976	Uruguay	Salto	−31.38	−57.95	33
		Punta del Este	−35	−55	16
DJF 1977	Cluster DJF-A	Lima-Callao/A	−12.00	−77.12	13
		Ayacucho	−13.13	−74.22	2749
		Pisco	−13.75	−76.28	7
		San Juan	−15.38	−75.17	60
		La Serena	−29.90	−71.20	142
		Punta Ángeles	−33	−71.70	41
		Puerto Montt	−41.42	−73.08	85
DJF 1977	Cluster DJF-B	Santo Domingo	18.43	−69.88	14
		Juliana Airport	18.05	−63.12	9
		Kingston/Norm	17.93	−76.78	14
		Le Raizet/Gua	16.27	−61.52	11
		Puerto Lempir	15.22	−83.80	13
		São Gabriel	−0.13	−67.08	90
		Guayaquil/Sim	−2.15	−79.88	9
		Talara	−4.57	−81.25	90
DJF 1978	Tropical SA	Bogotá/Eldora	4.72	−74.15	2548
		Yurimaguas	−5.90	−76.08	194
		Moyobamba	−6.03	−76.97	832
		Chachapoyas	−6.22	−77.83	2435
		Cajamarca	−7.13	−78.47	2622
		Juanjui	−7.22	−76.72	363
		Puerto Stroessner	−25.53	−54.60	196
DJF 1978 (Figure 3(f))	SSA (Argentina)	Mar del Plata	−37.93	−57.58	21
		Bariloche Aero	−41.15	−71.17	840
		Maquinchao	−41.25	−68.73	888
		Esquel Aero	−42.93	−71.15	785
		Trelew Aero	−43.2	−65.27	43
		Comodoro Rivadavia	−45.78	−67.5	46
		Puerto Deseado	−47.73	−65.92	80
		Río Gallegos	−51.62	−69.28	19
		Ushuaia Aero	−54.8	−68.32	14
		Punta Arenas	−53	−70.85	37
DJF 1979 (Figure 3(g))	SESA (Argentina–Uruguay)	Mercedes	−33.25	−58.07	17
		Azul Aero	−36.75	−59.83	132
		Neuquén Aero	−38.95	−68.13	271
		Bahía Blanca Aero	−38.7	−62.2	72
		San Antonio O	−40.78	−65.1	20
DJF 1978 (Figure 6(b))	Eastern Patagonia (Argentina)	Sarmiento	−45.60	−69.10	268
		Comodoro Rivadavia	−45.78	−67.5	46
		Santa Cruz Aero	−50.02	−68.57	111
		Río Gallegos	−51.62	−69.28	19

3.2. Precipitation

Figure 4(a) shows the difference of mean annual precipitation between 1961–1973 and 1978–1990 from UDel gridded data. Precipitation decreases along the equator, from there southwards until 15°S at the western coast of SA, and over the southwestern tip of SA. In contrast, more precipitation is observed east of the Andes mainly between 10°S and 30°S, i.e. over the cooling sub-Amazonian region and Bolivia. This pattern is also suggested by the sparse selected GHCN stations (Figure 4(c)). Mean shifts in UDel data and GHCN stations (Figure 4(b) and (d), respectively) are located in the regions mentioned above, with the exception of the southwestern tip of the continent, where precipitation changes are not due to a shift but to a negative trend, as described e.g. by Quintana and Aceituno (2012). Annual precipitation shifts in eastern Brazil exhibit a dipole around 10°S, with decrease to the north and increase to the south. Besides, there are some indications of abrupt precipitation increase over the Central region of Argentina, between 30°S and 40°S.

The DJF precipitation change pattern (figures not shown) exhibits a shift-like decrease to the north of the Amazon Basin (around the equator and 64°W), over western tropical SA (mainly Ecuador and Peru) and over southern Chile (around 44°S), whereas an abrupt precipitation increase is observed in the sub-Amazonian region and CWA, resembling the behaviour at annual level.

3.3. Pressure and geopotential height

We identify in both reanalyses three broad regions of abrupt decreases in mean annual SLP in 1975–1976 (Figure 5(a) and (b)): the North Pacific (centred around

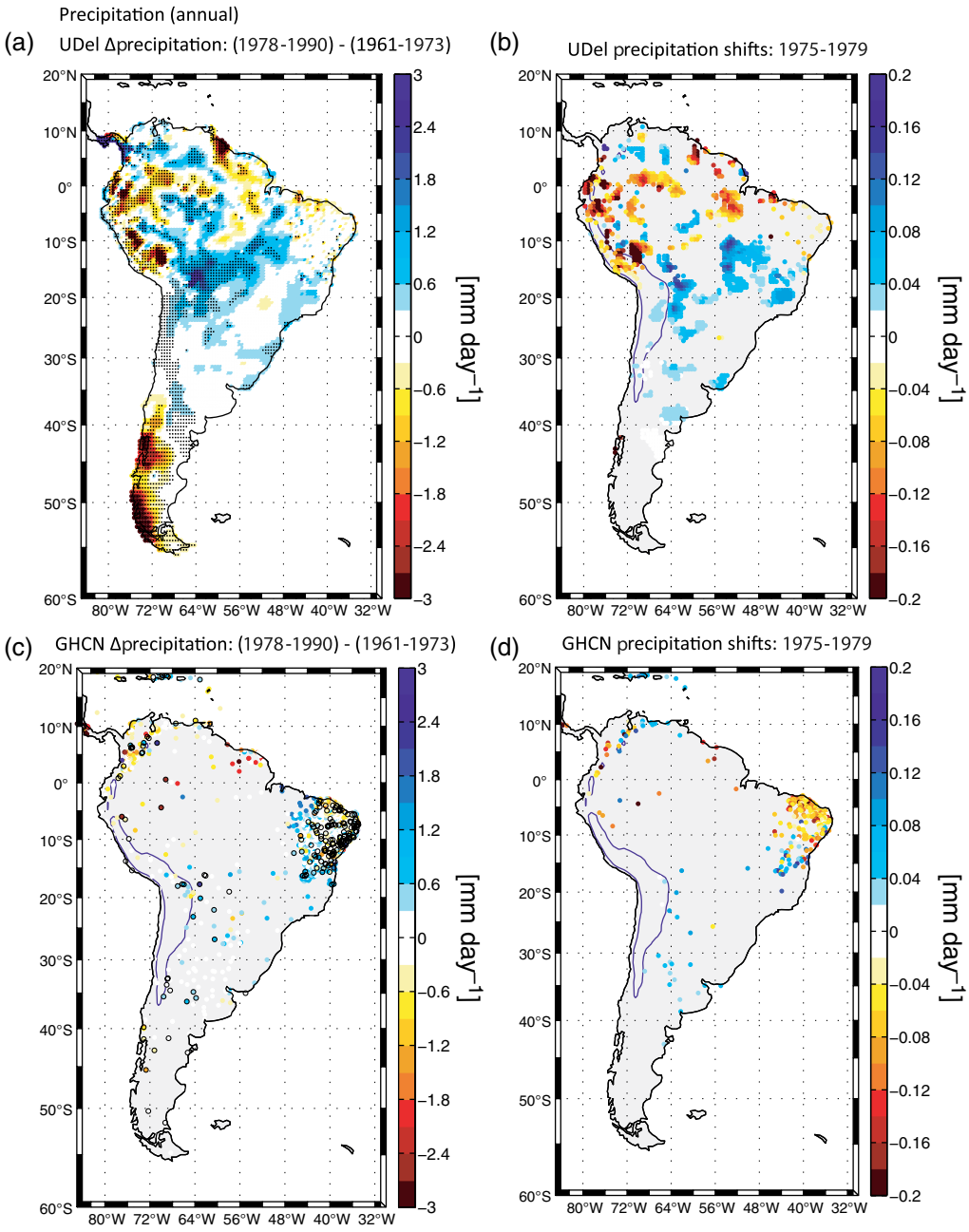

Figure 4. (Left panels) Annual mean precipitation difference (mm day^{-1}) between 1961–1973 and 1978–1990 from (a) UDel gridded data and (c) GHCN stations; statistically significant values (95%) are depicted by black dots. (Right panels) Precipitation shifts identified by Rodionov's test between 1975 and 1979, shown as differences between periods of 10 years before and 10 years after their detection, from (b) UDel gridded data and (d) GHCN stations. Over the continent, the solid contour depicts the 2000 m isoline.

60°N; 170°W, the area of the Aleutian Low); the Northeast Pacific (centred at 30°N; 130°W) and the Southeast Pacific (around 30°S; 110°W, the area of the SEPA). A positive SLP shift over the southern tip of SA is observed in 1975–1976 in NNR, but not in the shorter ERA-40 dataset. To analyse these regions, following composites were constructed: SEPA (25°–35°S; 100°–120°W) and SA Southern Tip (50°–55°S; 70°–75°W) (see Figure 5(a) and (b)).

The SLP shift-like decrease over the Southeast Pacific exhibits a clear signal in both reanalyses (Figure 5(c) and (d)), a fact that reflects the robustness of that phenomenon. Although the SLP time series from NNR shows a negligible trend in SEPA during 1950–2000, two periods of slightly positive trends separated by a shift of −2.66 hPa in 1975–1976 can be distinguished: 0.05 hPa year^{-1} for 1951–1975 and 0.06 hPa year^{-1} for 1976–2000. To further validate the reanalysis data, we included in Figure 5(c) and (d) the two GHCN instrumental records available for this almost data-void region, also discussed by Falvey and Garreaud (2009). The SLP time series of Easter Island (27°09′S; 109°25′W, 51 masl; standardized with respect to 1961–1990) shows excellent agreement with both SEPA composites. Although the corresponding time series at

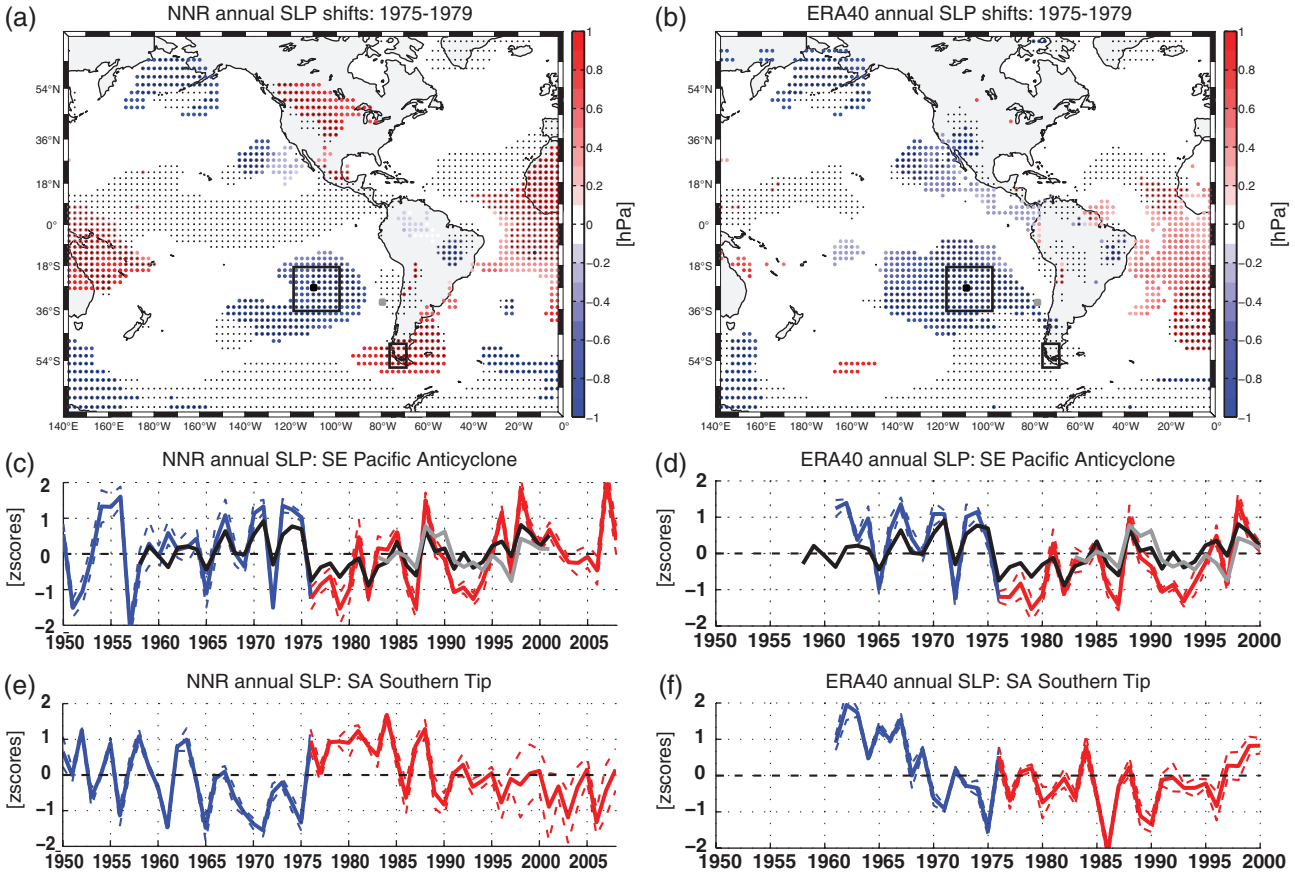

Figure 5. (Upper panels) SLP shifts identified through Rodionov's test between 1975 and 1979, shown as differences between periods of 10 years before and 10 years after their detection, from (a) NNR and (b) ERA-40. Statistically significant values (95%) of the mean SLP difference between 1961–1973 and 1978–1990 are depicted by black dots; the corresponding gridpoints do not necessarily show a shift in their time series and therefore are not necessarily colour-filled. (Lower panels) Time series of the composite mean ± 1 SD, standardized with respect to 1961–1990 (zscores), corresponding to the areas enclosed in (a–b): SEPA (25°–35°S; 100°–120°W) and South American Southern tip (50°–55°S; 70°–75°W), from (c, e) NNR, and (d, f) ERA-40. In panels (c–d) the standardized SLP time series of Easter Island (black curve; reference period: 1961–1990) and Juan Fernández (grey curve; reference period: 1983–2001) are also shown. Their locations are depicted by a black and a grey dot in panels (a and b), respectively.

Juan Fernández (33°40′S; 78°59′W, 30 masl; standardized with respect to 1983–2001) exhibits a similar interannual variability as that from Easter Island, its negligible trend indicates that the strengthening of the high pressure cell detected around the center of the SEPA weakens beyond its eastern edge.

The anticyclonic anomaly observed in NNR over the southern tip of SA from 1976 onwards is less evident in ERA-40 (Figure 5(e) and (f)). A general characteristic for SLP differences is that they are more prominent for DJF than for the annual means. In DJF 1978, SLP abruptly increases over the South Atlantic Ocean and in the continent over SESA (31°–36°S; 58°–64°W), as registered by reanalysis data and GHCN records (not shown).

3.4. Geopotential height and temperature in higher levels

To explore the manifestation of the shift at different heights, we have also assessed NNR data at 850, 700 and 500 hPa (figures not shown). Over SA at 850 hPa, we observe a positive geopotential height shift over the southern half of the continent, more intense towards its southern tip, and notorious warming (>1 °C) over La Plata Basin and at mid-latitudes. At 700 and 500 hPa, shift-like increases of geopotential height and air temperature are detected over the northern, subtropical and southernmost regions of the continent.

Over the Pacific Ocean at 850 hPa, we identify a subtle but abrupt increase of geopotential height in the tropics. A decrease of this variable over the SEPA area is observed around 25°S; 100°W, but its pattern is spatially more reduced compared with the one of SLP and does not occur as a shift in the mean. Also at 850 hPa, a warming shift is observed in the tropics, in front of the Chilean coast (ca. 18–50°S, extending to the West over the South Pacific Ocean until approximately 110°W), and then again more to the South, between roughly 45°S and 60°S. At 700 hPa, however, although the warming shift is still observed in the tropics and the zonal belt in the South, the signal is confined over the continent and along the coast between 18°S and 36°S, but does not extend further into the Pacific Ocean anymore. At 500 hPa, the shift-like warming pattern is similar to that observed at 700 hPa, although the signal gets lost in the central and eastern tropical Pacific.

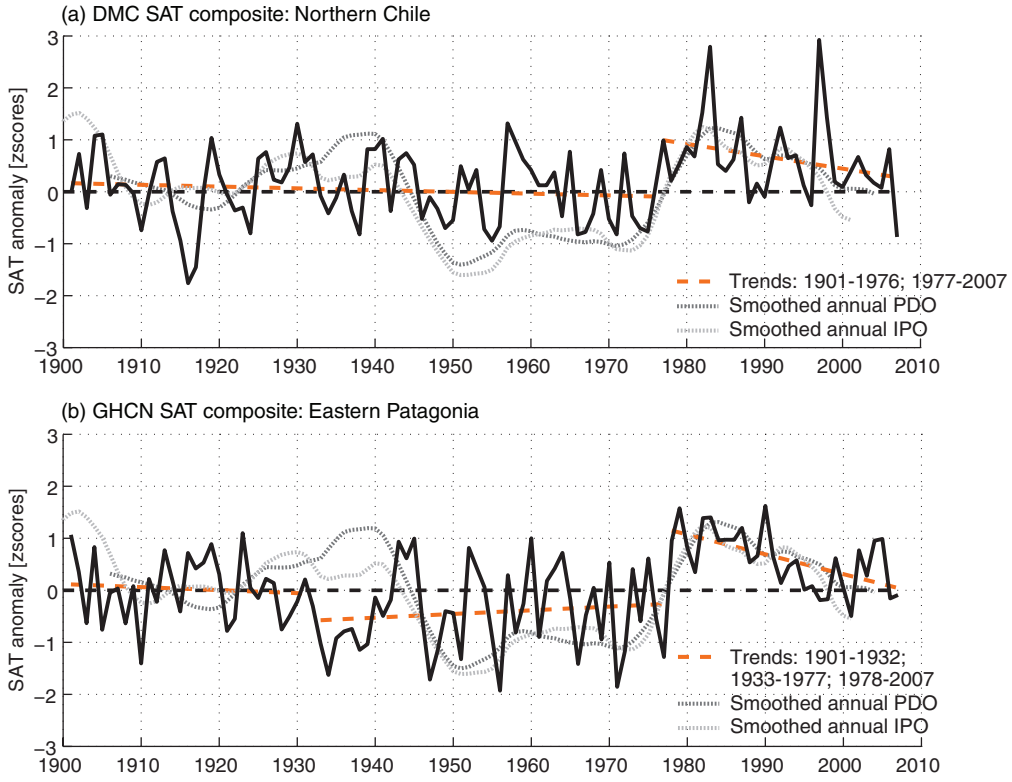

Figure 6. (a) Annual long-term SAT composite, standardized with respect to 1950–1979 (zscores), of three stations situated along the arid coast of northern Chile showing a shift in 1977 (Source: Schulz *et al.* (2012)). (b) DJF long-term SAT composite, standardized with respect to 1950–1979 (zscores), of four stations located in eastern Patagonia showing a shift in 1978 (GHCN gaps in 1902 and 1991 have been filled using a regression on UDel gridded data; this composite is comparable with the one shown in Figure 3(f)). For station details, see Tables 1 and 2. The dashed dark grey (dashed light grey) curve corresponds to the smoothed annual PDO (IPO) index, obtained by applying a 7-year running mean twice, and scaled to the amplitude of the SAT composites.

4. Discussions

4.1. Interpretation of the SEPA shift

The prominent abrupt SLP decrease over the southeast Pacific in 1975–1976 (Figure 5(a) and (b)) appears as a key factor to explain the shifts observed in SST and eventually also in SAT. Our interpretation is that the weakening of SEPA induced an anomalous cyclonic circulation centred around 30°S; 110°W, implying a negative anomaly of the southerly (southeasterly) wind intensity at its eastern (northeastern) flank at both DJF and annual levels, leading consequently to a weakening of the strength of the Humboldt system, which maintains relatively cold local conditions. Therefore, in a large-scale sense, a weaker northward cold current along the southwestern coast of SA might have been expected after the 1970s climate shift. This would have contributed at least partly to the warm SST shift observed there. Such an interpretation is similar but of opposite polarity to the strengthening of the warm advection along the western coast of North America due to a more intense Aleutian Low after the 1970s shift (Trenberth, 1990), a pattern also detected in our ENSO-filtered SST series over the Northeast Pacific (not shown). In this context, Pizarro and Montecinos (2004) found a deeper thermocline over the Eastern South Pacific Ocean after the 1970s shift, reflecting warmer SST along the southwestern South American coast. In addition, Quintana and Aceituno (2012) described the phase opposition at interdecadal timescales between the SEPA intensity and the index of the Interdecadal Pacific Oscillation (IPO, Power *et al.*, 1999). Consequently, along with the decreasing values of the IPO and PDO indices during the last decades (Figure 6), the intensity of the SEPA has been strengthening (Falvey and Garreaud, 2009; Quintana and Aceituno, 2012), a phenomenon that is consistent with the observed positive (negative) trend of local SLP (SAT) records documented here and in cited works.

4.2. Factors associated with the precipitation change pattern

The pattern of annual precipitation change around mid-1970s (Figure 4(a)) features a dry anomaly in the northern part of SA and a wet anomaly south of 10°S, including some regions in the subtropics. These changes are comparable to the regression pattern associated with the warm PDO phase and, due to the subtler anomaly observed in the subtropics, to a lesser extent with the warm ENSO phase (fields presented by Garreaud *et al.* (2009)). Nevertheless, an outstanding exception is the extensive dry anomaly over southwestern SA. Huang *et al.* (2005) showed previously a clear resemblance between the post-minus pre-1976 January–May precipitation change and the ENSO-induced response of this variable. This similarity between interdecadal and interannual patterns of

precipitation variability could be partially explained by the fact that the ENSO-related precipitation signal over SA is more conspicuous during warm PDO phases (Andreoli and Kayano, 2005; Kayano *et al.*, 2009). In line with this result, Haylock *et al.* (2006) pointed out that the two large-scale changes that accounted for the precipitation variability over SA during 1960–2000 were (1) a trend towards more negative Southern Oscillation Index (SOI) values and (2) a weakening of the continental SLP trough in SSA, which induces a shift of the storm track to the South.

A factor that could have caused the observed DJF precipitation change pattern over the southern Amazon region and CWA around mid-1970s is the intensification of the meridional low-level jet from the humid lowlands of Brazil and Bolivia, leading to more moisture advection after the shift (Compagnucci *et al.*, 2002). Besides, Carvalho *et al.* (2011), based on NNR, showed that the South American Monsoon System exhibited a longer duration after the 1970s climate transition, due to both an earlier onset and a later demise. Analysing the difference between the period after the shift minus the period before it during DJF (the peak months of the monsoon system), they found a westerly anomaly in the tropics in the vertically integrated moisture flux, which advects moisture from the tropical Pacific into the continent and is then deflected southward towards a cyclonic anomaly over central Brazil and southern Amazonia. It is worth noting that the circulation anomalies described by them after the shift (their Figure 8), also including other features discussed in our paper, such as the anticyclonic anomaly in the southern tip of the continent (Figure 5), are in good agreement with the low-level circulation changes reported below in the present work (Figure 7(a)–(c)). More to the south, sedimentological proxies from Laguna Mar Chiquita in SESA (Piovano *et al.*, 2002) further indicate the regional robustness of this large wet anomaly after the 1970s climate shift. On the other hand, Gonzalez *et al.* (2014) recently ascribed the positive summer precipitation trend of SESA during 1960–2000 to circulation changes due to stratospheric ozone depletion.

4.3. Role of ENSO in the temperature shift

The interannual variability of climate can be affected by abrupt changes in the background circulation. On the other hand, climate regime changes may be triggered by the varying frequency of interannual phenomena. Therefore, it is worth analysing to which extent the ENSO-related variability had an impact in the regime shift signal of mid-1970s. One way to explore this aspect is by removing the ENSO signal from the analysed time series of SST and SAT. For this, we use here two alternative methodologies. As a first approach, we calculate SAT differences of the GHCN composites of Figure 3 between 1965–1975 and 1980–1990 considering two groups of data: (1) taking into account all years and (2) selecting just ENSO-neutral years by removing those identified as El Niño (1966, 1973, 1977, 1983, 1987) or La Niña (1968, 1971, 1974, 1976, 1985, 1989). The calculated magnitudes of ΔSAT (standardized values) are shown in Figure 3 by the numbers in the upper-left corner of each panel. These results point to a prominent temperature difference considering just ENSO-neutral years and indicate the existence of the shift beyond the variability associated with this interannual mode.

Next, we applied following alternative procedure to the SST and SAT gridded data: (1) subtraction of the 1950–2000 least-squares linear trend of each gridpoint, (2) regression of the detrended time series on the Niño3.4 annual index and (3) calculation of the residual series by removing the values obtained after step 2 from those calculated in step 1. The ENSO-filtered SST composites of Figure 1(e) and (f) were obtained in this way. The Equatorial Pacific composite shows strongly damped interannual variability and no shift, whereas the Southeast Pacific composite exhibits a residual SST shift in the late 1970s. This is in agreement with Montecinos *et al.* (2003), who showed that the SST variability along the western coast of SA during the second half of the 20th century reveals two main modes: ENSO and the interdecadal variability. In our case, ENSO-filtered SST time series from the South Pacific exhibit shift-like warming just along the southwestern coast of the continent (from 10°S to 45°S) and to the north and the east of the SEPA (figures not shown). Besides, shift-like cooling in the ENSO-filtered SST time series is detected around 40°S; 100–120°W, to the southwest of the SEPA. Both features, interpreted as anomalies of temperature advection, indicate a weakening in the intensity of the circulation associated with the SEPA system.

Over the continent, the results obtained using non-filtered UDel SAT data (not shown) agree with the analysis of GHCN SAT annual means (Figure 2(a)): shifts are observed along the western coast of SA, Venezuela and SESA. On the other hand, ENSO-filtered annual SAT series show that the shift signal persists just along the western coast of SA, specifically in Central and northern Chile (20°–40°S) and in northern Peru, around 8°S.

In the case of summer series, nonfiltered DJF SAT data from UDel exhibit the abrupt warming along the northwestern coast of the continent (Peru and southern Colombia), in northern Chile (ca. between 23° and 28°S) and over SSA (Patagonia, south of 35°S). In the ENSO-filtered DJF SAT series, the shift signal persists just between 40°S and 50°S. Since the ENSO imprint has been removed from these records, this result indicates that factors other than this interannual mode must play a role in the local manifestation of this abrupt warming.

4.4. The summer warming in SSA

We found that summer warming around the shift is highest in eastern SSA. In the case of SESA, the abrupt SLP increase detected in summer 1978 agrees with the results of Barros *et al.* (2008), who documented the southward shift of the southwestern part of the South Atlantic Anticyclone during the warm semester (October–March) and showed that the second principal component of SLP exhibits an

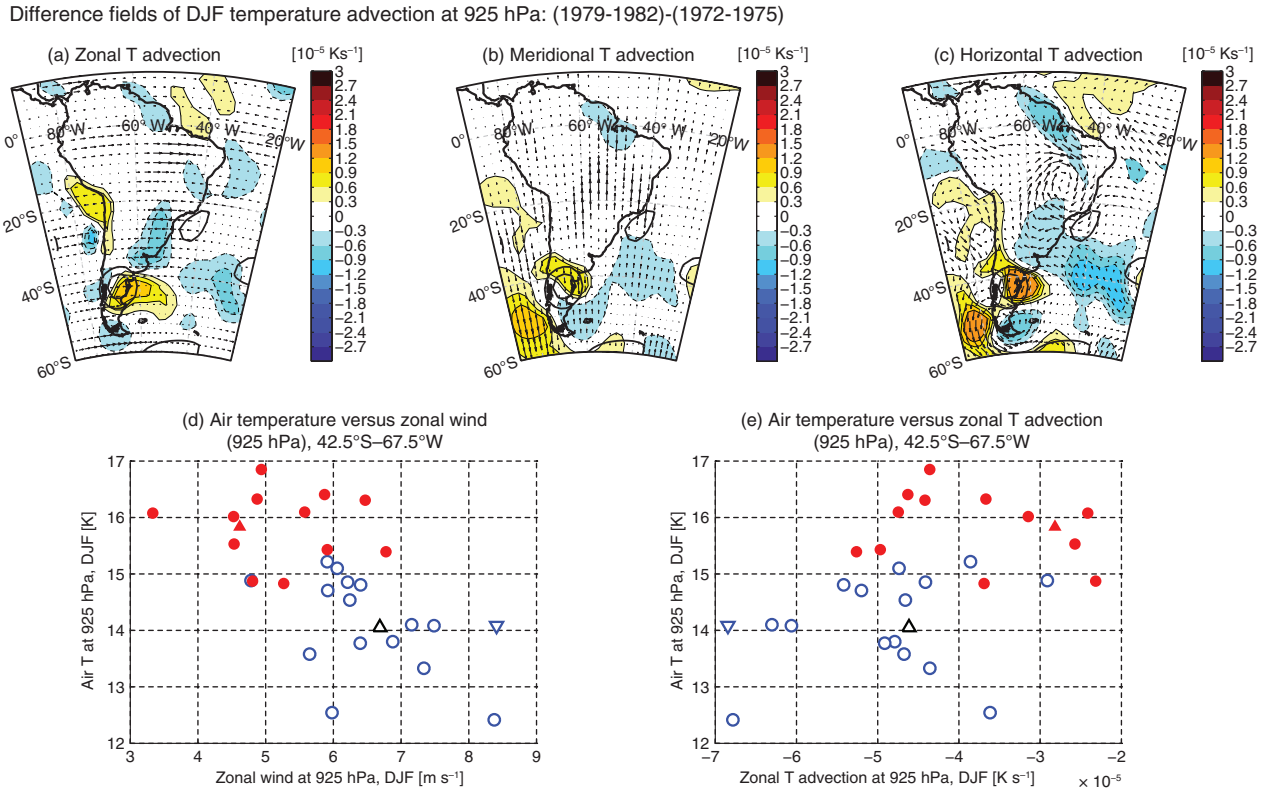

Figure 7. (Upper row) Difference fields of DJF temperature advection (10^{-5} K s^{-1}) (different contours) by the mean flow (vectors) at 925 hPa between 1972–1975 and 1979–1982, derived from NNR: (a) zonal component, (b) meridional component, and (c) total horizontal temperature advection, i.e. the sum of the zonal and meridional components. Thin solid/dashed contours denote positive/negative values (see colour scale); thick black contours show the air temperature change every 0.5°C, starting at 1°C. (Lower row) Scatter plots of (d) air temperature *versus* zonal wind and (e) air temperature *versus* the zonal component of the horizontal temperature advection, both at 42.5°S; 67.5°W and 925 hPa. Empty blue and filled red circles are used for 1962–1975 and 1979–1990, respectively. The inverted empty blue triangle depicts 1976, the non-inverted empty black triangle stands for 1977, and the non-inverted filled red triangle indicates 1978.

abrupt increase in 1978 (see their Figure 9). This SLP increase could eventually be related to the summer warming observed over SESA (Figure 2(d)), which might have been caused hypothetically by enhanced subsidence and clearer skies after the shift.

On the other hand, in the southern part of SSA, air temperature from NNR at 925 hPa and 42.5°S; 67.5°W is negatively correlated with zonal wind and positively correlated with horizontal temperature advection (Figure 7(d) and (e)). Although the low-level temperature advection is always negative and mainly zonal during DJF, after the shift its intensity weakens, partly due to the southward-shift of the westerlies (Figure 7(a)–(c)). This result implies a net warming and probably less cloudiness after mid-1970s, which could have led to stronger solar radiation over this area.

4.5. The warming in northern Chile

The signal found along northern Chile agrees with the results of Schulz *et al.* (2012), who, based on radiosonde data from Antofagasta (23°26′S; 70°26′W), showed a cold-to-warm transition throughout the troposphere in mid-1970s. Their study reported that the warming trend above the temperature inversion layer (TIL) became stronger after the shift, whereas a significant cooling took place below the TIL. Moreover, using observations from northern Chile, they documented a decline of total cloud cover (mainly stratocumuliform there) and of cloudy days around 1976–1977. In agreement, Clement *et al.* (2009) showed that mid-level marine cloud cover along the coast of northern Chile and southern Peru (in particular its stratiform component) seems to be anticorrelated at interdecadal scale with SST in the Northeast Pacific. Hence, the 1970s shift could have been associated with a decrease in mid-level cloud cover. This fact allows the speculation of enhanced net shortwave radiation to the surface leading to warming after the 1970s shift. Indeed, surface fluxes retrieved from NNR for the Southeast Pacific along the coast of northern Chile (20°S–30°S; 72.5°W–77.5°W) show at annual (DJF) level a mean increase in net shortwave radiation of 10.2 W m^{-2} (4.8 W m^{-2}) between 1961–1973 and 1978–2000 and, in the case of sensible heat net flux, of 1.9 W m^{-2} (2.3 W m^{-2}). In this region, the maximum correlation between SAT measured at coastal stations and contiguous gridded SST occurs at no lag at monthly scale, as shown by cross-correlation analysis by Jacques (2009). The tight local connection between SST and maximum SAT could be partly due to temperature advection by the prevailing sea-land breeze during daytime.

Off northern Chile and southern Peru, the SEPA dominates the large-scale wind-stress field (Bakun and Nelson, 1991) and therefore a decrease in its intensity would be associated with a weaker forcing leading to coastal upwelling. However, Pizarro *et al.* (1994) showed that other factors should be considered to determine the regional and local wind stress field, such as the thermal contrast between the ocean and the hyperarid coast. They found a good agreement between the annual wind cycle and the wind stress field in Iquique (21°20′S), but not in Arica (18°28′S) nor Antofagasta (23°38′S). While Narayan *et al.* (2010) reported a significant decrease of upwelling off southern Peru after 1960 from an SST index and comment on the association with the transition from predominantly La Niña to El Niño conditions in mid 1970s, Gutiérrez *et al.* (2011) and Vargas *et al.* (2007) describe the enhancement of coastal upwelling off southern Peru since the 1950s and off Antofagasta during El Niño-like conditions, respectively. Thus, Gutiérrez *et al.* (2011) encourage future research aiming at understanding the distinct impacts on coastal upwelling of the SEPA spin-up observed during recent decades (Falvey and Garreaud, 2009) and the enhancement of the land-sea thermal gradient mechanism (Bakun, 1990).

4.6. Previous manifestations of SAT shifts

As a final exercise, we explore the occurrence of earlier SAT shifts in SA during the 20th century. For that, we select two regions where the 1970s shift in this variable is evident. One of them corresponds to the arid coast of northern Chile, whose composite is shown in Figure 6(a) (Table 1) together with smoothed annual indices of the PDO and the IPO. Although the Rodionov *t*-test detects warming (cooling) shifts in 1925 and 1976 (1914 and 1966), the magnitude of the last event is unprecedented in the record. Thus, we can model the composite series as two cooling trends ($-0.02\,^{\circ}\mathrm{C\,decade^{-1}}$ for 1901–1976 and $-0.11\,^{\circ}\mathrm{C\,decade^{-1}}$ for 1977–2007) separated by a shift in 1976, whose magnitude can be estimated as the local difference of both trends: $\Delta\mathrm{SAT}_{1976} = 0.52\,^{\circ}\mathrm{C}$. The composite of northern Chile seems to be modulated by PDO/IPO during the second half of the 20th century, whereas this relationship does not appear clearly during the preceding decades. This observation is supported by the variance fraction of the composite explained by the annual PDO index during 1906–1955 (∼9%) and 1956–2004 (∼25%).

The second region is eastern Patagonia, where a DJF SAT shift stands out in 1978 (see Table 2 and Figure 6(b)). The summer SAT variability in this region during the 20th century was explored in detail by Jacques-Coper and Brönnimann (2014). In this composite, Rodionov's test detects also a weaker warm-to-cold transition in 1933 and not in the late 1940s, as expected from a PDO-driven interdecadal variability. If we model this series as a sequence of trends within three periods ($-0.06\,^{\circ}\mathrm{C\,decade^{-1}}$ for 1901–1932, $0.07\,^{\circ}\mathrm{C\,decade^{-1}}$ for 1933–1977 and $-0.36\,^{\circ}\mathrm{C\,decade^{-1}}$ for 1978–2007), we can calculate the magnitudes of the SAT shifts in 1933 and 1978 as in previous case: $\Delta\mathrm{SAT}_{1933} = -0.48\,^{\circ}\mathrm{C}$ and $\Delta\mathrm{SAT}_{1978} = 1.33\,^{\circ}\mathrm{C}$. Again, the PDO index explains a greater amount of the total variance of the temperature composite during 1956–2004 (∼38%) than during 1906–1955 (∼2%).

Given the outstanding magnitude of the 1970s shift in both locations, we agree with Agosta and Compagnucci (2008) and conclude that its associated effects seem to be unprecedented during the 20th century.

The second conclusion from our results is that the PDO seems to have had a variable impact on SAT in the selected locations during the 20th century. To put these two regions in a continental context, we calculated the correlation coefficients between the interdecadal component of the mean annual PDO index and the interdecadal component of mean annual UDel SAT at every gridpoint within SA for the periods (a) 1906–1950, (b) 1958–2002 and (c) 1906–2002 (Figure 8). The interdecadal components were calculated as follows: (1) detrending of the annual mean time series and (2) application of a 7-year running mean twice, which reduces the length of the time series by 6 years at the edges, resulting in a final total length of 97 years within 1906–2002. Interestingly, Figure 8(b) shows that the correlation pattern for 1958–2002 (which comprises the period of analysis of the time series in the first part of our paper, 1961–1990) resembles the SAT changes and shifts detected around late 1970s. In other words, the PDO interdecadal variability can be related to the interdecadal SAT modulation over most of the regions discussed in this study during the second half of the 20th century (compare Figure 8(b) with Figure 2(a)). Moreover, the positively-correlated areas exhibit good agreement with those which show a warming shift around 1970s (Figure 2(b) and (d)), in particular the southwestern coast of SA and Patagonia. Nevertheless, the corresponding correlation pattern during the first half of the 20th century (1906–1950, Figure 8(a)) shows a very different structure. Although the observational data from which the interpolated UDel product is derived become much scarcer during that period, we observe that this early pattern is consistent with our findings from the instrumental composites of northern Chile and Patagonia, which do not exhibit a clear PDO-related signal within those years. The most prominent region which seems to hold a stable correlation with the PDO in the 20th century is the coast of Peru. As a result of this apparent instability in the interdecadal relationship between PDO and SAT on the continent, the correlation coefficient pattern for the whole period, 1906–2002 (Figure 8(c)), shows a less robust structure than their corresponding subperiods.

5. Conclusions

In this study we have addressed the mid-1970s climate shift over SA, showing its spatial patterns and related magnitudes. Initially detected in SST over the Pacific Ocean, it is also observed over the continent in SAT, precipitation, and SLP records. A conceptual scheme of

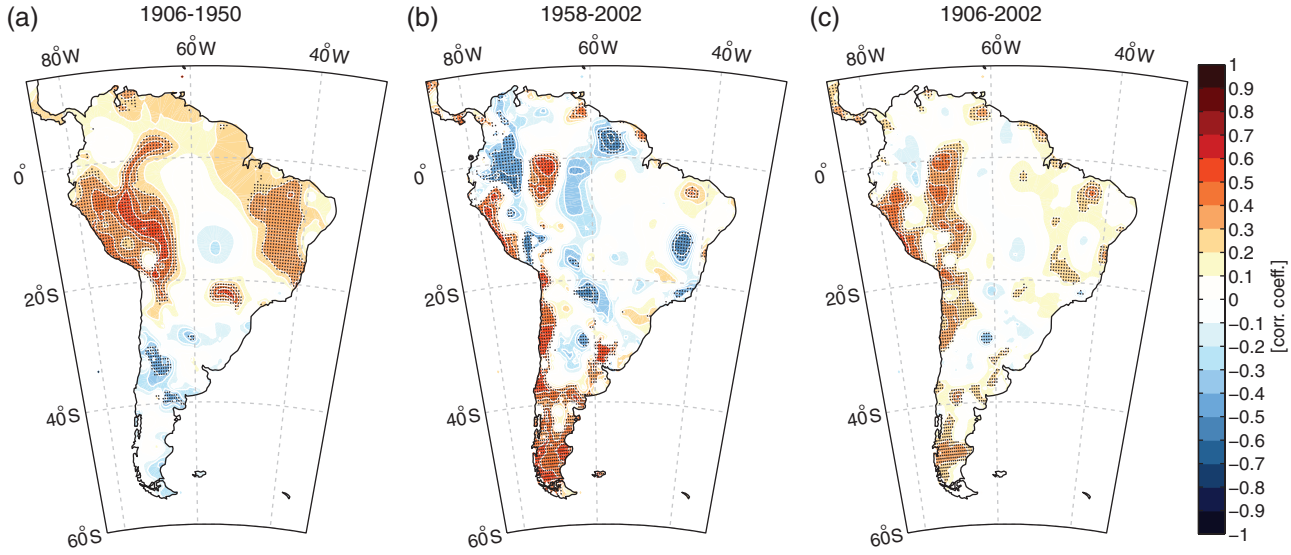

Figure 8. Correlation coefficients between the interdecadal component of the mean annual PDO index and the interdecadal component of mean annual UDel SAT at every gridpoint within SA for the periods (a) 1906–1950, (b) 1958–2002 and (c) 1906–2002. Black dots denote statistically significant values at 90%, accounting for autocorrelation in the time series after Bretherton *et al.* (1999).

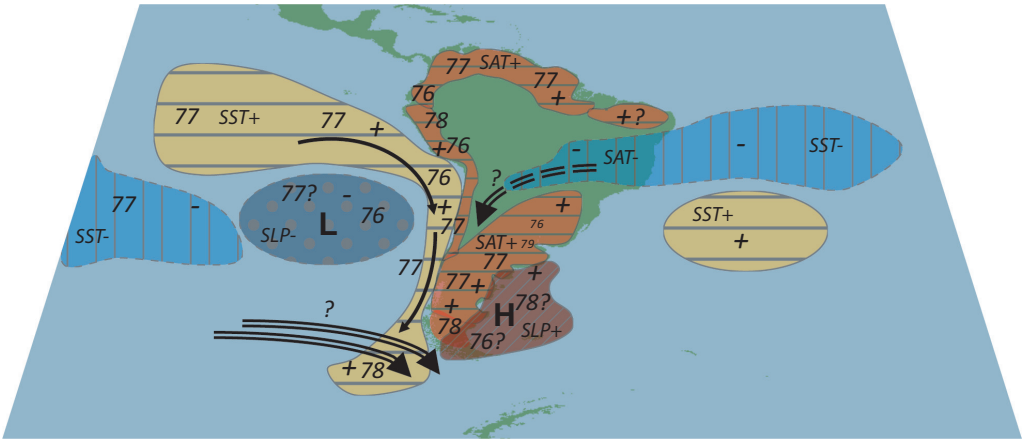

Figure 9. Conceptual scheme of changes related to the climate shift of the 1970s in South America at annual level. Anomalies are shown with their corresponding sign and year of detection: oceanic/atmospheric circulation by single/double arrows, SLP (positive/negative values depicted by diagonal hatching/dotted pattern), SAT, and SST (positive/negative values depicted by horizonal/vertical hatching).

the associated anomalies is proposed in Figure 9. The shift signal for these variables is detected at different years over different regions, which indicates that the events are not synchronous. This could be explained by a delay in the propagation of the ocean signal into the atmosphere over the continent. Nevertheless, the cause behind the temporal sequence of the shifts lies beyond the aims of this article.

We first observe the cold-to-warm transition pattern in SST, a phenomenon that has been previously related to the PDO. Over the continent, SAT exhibits warming in regions located next to the Pacific Ocean, the northern coast of SA, the Caribbean, and SESA, contrasting with the cooling observed over the Gran Chaco region around 20°S. In the Southeast Pacific, along the coast of northern Chile, the warming pattern could be related to less local cloudiness after the shift. As a possible precursor of all these anomalies, we identify the shift-like weakening of the SEPA intensity in 1976. This anomalous circulation seems to have weakened the Humbold current system, which normally maintains local cold conditions. This result agrees with the phase opposition between the intensity of the SEPA and the index of the IPO reported by Quintana and Aceituno (2012). During the last decades, however, a positive SLP trend reveals the strengthening of the SEPA, thus enhancing the cold conditions along the southwestern coast of the continent. This phenomenon has been observed in simulations and described as a consequence of global warming (Falvey and Garreaud, 2009). Alternatively, it could be interpreted, at least partially, as a readjustment of the system after the mid-1970s perturbation. We have also focused on the austral summer season because of its pronounced SAT signals. Over SSA at mid-latitudes, summer temperature series show an abrupt increase in 1978, partially explained by reduced cold horizontal temperature advection after the shift due to southward-shifted westerlies.

Many effects related to the 1970s shift are located in regions where the ENSO relationships have been well established and are consistent with a higher frequency of warm ENSO events after this abrupt climate change. Since the signal of the SAT shift remains in some areas after filtering the ENSO-related variability of the time series, we subscribe to the conclusion of previous studies and suggest that other factors, in particular low-frequency variability, must have also played a role in its manifestation. Thus, an alternative view is that a low frequency mode such as the PDO or the IPO has modulated the interannual variability, at least during the last decades, and was then the main driver of the shift. In this respect, Yasunaka and Hanawa (2005) showed that both ENSO and PDO suffered a regime shift in the mid-1970s and that, in general, regime shifts occur in phase with ENSO events, a fact that could explain the pronounced observed DJF signals.

Due to its characteristics, the 1970s climate shift appears as an unprecedented event during the 20th century over SA. In particular, the 1970s SAT shift is robust and stands out as an isolated manifestation in the century-long instrumental SAT records of northern Chile and eastern SSA. Our results suggest that, at interdecadal scale, annual SAT over most of the continent does not show a stable relationship with the PDO index. Thus, we question the quite traditional paradigm of understanding PDO as a low-frequency variability mode of SAT in SA. In this context, the absence of a clear relationship between phase changes of the PDO and the IPO and preceding climate shifts deserves further research, for which good quality long-term records are needed.

Acknowledgements

The authors would like to acknowledge the availability of the Matlab script of Rodionov's sequential *t*-test (www.beringclimate.noaa.gov), the Niño3.4 index (http://www.cgd.ucar.edu/cas/catalog/climind/TNI_N34/index.html#Sec5), the PDO index (http://jisao.washington.edu/pdo/PDO.latest) and the IPO index (www.iges.org/c20c/IPO_v2.doc). GHCN-Monthly version 2 provided by NOAA's National Climatic Data Center (http://www.ncdc.noaa.gov/ghcnm/v2.php). UDel data were downloaded from http://climate.geog.udel.edu/~climate/html_pages/archive.html. NCEP Reanalysis and NOAA_ERSST_V3 data provided by the NOAA/OAR/ESRL PSD, Boulder, CO, USA, from their Web site (http://www.esrl.noaa.gov/psd/). ECMWF ERA-40 data used in this study have been obtained from the ECMWF Data Server (http://data-portal.ecmwf.int/). The HadISSTv1 dataset was provided by the MetOffice Hadley Center, Exeter, UK, from their Web site (http://www.metoffice.gov.uk/hadobs/hadisst/data/download.html). We express our gratitude to Prof. Patricio Aceituno, Prof. Aldo Montecinos, and Prof. José Rutllant for constructive discussions. Many thanks to Dr Fabia Hüsler, Dr Alexander Stickler, Dr Renate Auchmann, Dr Isabel Moreno and Dr Iván Hernández-Almeida, who kindly supported the preparation of the manuscript. This work has benefited from the enriching comments and suggestions of two anonymous reviewers. MJC was financed by the ACT-19 project during the realization of this study and by the BecasChile scholarship programme during the final redaction of this paper (CONICYT-Chile). RG was partially supported by FONDAP-CONICYT1511 0009 (CR2).

References

Agosta EA, Compagnucci RH. 2008. The 1976/77 austral summer climate transition effects on the atmospheric circulation and climate in southern South America. *J. Clim.* **21**: 4365–4383, doi: 10.1175/2008JCLI2137.1.

Andreoli RV, Kayano MT. 2005. ENSO-related rainfall anomalies in South America and associated circulation features during warm and cold Pacific Decadal Oscillation regimes. *Int. J. Climatol.* **25**: 2017–2030, doi: 10.1002/joc.1222.

Bakun A. 1990. Global climate change and intensification of coastal ocean upwelling. *Science* **247**: 198–201, doi: 10.1126/science.247.4939.198.

Bakun A, Nelson CS. 1991. The seasonal cycle of wind-stress curl in subtropical eastern boundary current regions. *J. Phys. Oceanogr.* **21**: 1815–1834, doi: 10.1175/1520-0485(1991)021<1815:TSCOWS>2.0.CO;2.

Barros VR, Doyle ME, Camilloni IA. 2008. Precipitation trends in southeastern South America: relationship with ENSO phases and with low-level circulation. *Theor. Appl. Climatol.* **93**: 19–33, doi: 10.1007/s00704-007-0329-x.

Bretherton CS, Widmann M, Dymnikov VP, Wallace JM, Bladé I. 1999. The effective number of spatial degrees of freedom of a time-varying field. *J. Clim.* **12**: 1990–2009, doi: 10.1175/1520-0442(1999)012<1990:TENOSD>2.0.CO;2.

Carvalho LMV, Jones C, Silva AE, Liebmann B, Silva Dias PL. 2011. The South American Monsoon System and the 1970s climate transition. *Int. J. Climatol.* **31**: 1248–1256, doi: 10.1002/joc.2147.

Chao Y, Ghil M, McWilliams JC. 2000. Pacific interdecadal variability in this century's sea surface temperatures. *Geophys. Res. Lett.* **27**: 2261–2264, doi: 10.1029/1999GL011324.

Chavez FP, Ryan J, Lluch-Cota SE, Ñiquen MC. 2003. From anchovies to sardines and back: multidecadal change in the Pacific Ocean. *Science* **299**: 217–221, doi: 10.1126/science.1075880.

Chen J, Del Genio AD, Carlson BE, Bosilovich MG. 2008. The spatiotemporal structure of twentieth-century climate variations in observations and reanalyses. Part II: pacific pan-decadal variability. *J. Clim.* **21**: 2634–2650, doi: 10.1175/2007JCLI2012.1.

Clement AC, Burgman R, Norris JR. 2009. Observational and model evidence for positive low-level cloud feedback. *Science* **325**: 460–464, doi: 10.1126/science.1171255.

Collins JM, Chaves RR, da Silva Marques V. 2009. Temperature variability over South America. *J. Clim.* **22**: 5854–5869, doi: 10.1175/2009JCLI2551.1.

Compagnucci RH, Agosta EA, Vargas WM. 2002. Climatic change and quasi-oscillations in central-west Argentina summer precipitation: main features and coherent behaviour with southern African region. *Clim. Dyn.* **18**: 421–435, doi: 10.1007/s003820100183.

Deser C, Alexander MA, Timlin MS. 1996. Upper-ocean thermal variations in the North Pacific during 1970–1991. *J. Clim.* **9**: 1840–1855, doi: 10.1175/1520-0442(1996)009<1840:UOTVIT>2.0.CO;2.

Deser C, Phillips AS, Alexander MA. 2010. Twentieth century tropical sea surface temperature trends revisited. *Geophys. Res. Lett.* **37**: L10701, doi: 10.1029/2010GL043321.

Falvey M, Garreaud RD. 2009. Regional cooling in a warming world: recent temperature trends in the southeast Pacific and along the west coast of subtropical South America (1979–2006). *J. Geophys. Res. Atmos.* **114**: D04102, doi: 10.1029/2008JD010519.

Garreaud R, Battisti DS. 1999. Interannual (ENSO) and interdecadal (ENSO-like) variability in the Southern Hemisphere tropospheric circulation. *J. Clim.* **12**: 2113–2123, doi: 10.1175/1520-0442(1999)012<2113:IEAIEL>2.0.CO;2.

Garreaud RD, Vuille M, Compagnucci R, Marengo J. 2009. Present-day South American climate. *Palaeogeogr. Palaeoclimatol. Palaeoecol.* **281**: 180–195, doi: 10.1016/j.palaeo.2007.10.032.

Giese BS, Urizar SC, Fučkar NS. 2002. Southern Hemisphere origins of the 1976 climate shift. *Geophys. Res. Lett.* **29**: 1–4, doi: 10.1029/2001GL013268.

Gonzalez PM, Polvani L, Seager R, Correa GP. 2014. Stratospheric ozone depletion: a key driver of recent precipitation trends in South Eastern South America. *Clim. Dyn.* **42**: 1775–1992, doi: 10.1007/s00382-013-1777-x.

Graham NE. 1994. Decadal-scale climate variability in the tropical and North Pacific during the 1970s and 1980s: observations and model results. *Clim. Dyn.* **10**: 135–162, doi: 10.1007/BF00210626.

Gutiérrez D, Bouloubassi I, Sifeddine A, Purca S, Goubanova K, Graco M, Field D, Méjanelle L, Velazco F, Lorre A, Salvatteci R, Quispe D, Vargas G, Dewitte B, Ortlieb L. 2011. Coastal cooling and increased productivity in the main upwelling zone off Peru since the mid-twentieth century. *Geophys. Res. Lett.* **38**: L07603, doi: 10.1029/2010GL046324.

Hartmann B, Wendler G. 2005. The significance of the 1976 pacific climate shift in the climatology of Alaska. *J. Clim.* **18**: 4824–4839, doi: 10.1175/JCLI3532.1.

Haylock MR, Peterson TC, Alves LM, Ambrizzi T, Anunciação YMT, Baez J, Barros VR, Berlato MA, Bidegain M, Coronel G, Corradi V, Garcia VJ, Grimm AM, Karoly D, Marengo JA, Marino MB, Moncunill DF, Nechet D, Quintana J, Rebello E, Rusticucci M, Santos JL, Trebejo I, Vincent LA. 2006. Trends in total and extreme South American rainfall in 1960–2000 and links with sea surface temperature. *J. Clim.* **19**: 1490–1512, doi: 10.1175/JCLI3695.1.

Huang H-P, Seager R, Kushnir Y. 2005. The 1976/77 transition in precipitation over the Americas and the influence of tropical sea surface temperature. *Clim. Dyn.* **24**: 721–740, doi: 10.1007/s00382-005-0015-6.

Jacques M. 2009. *Caracterización del salto climático de mediados de los 1970s en Sudamérica*, MSc thesis, Universidad de Chile, Santiago de Chile.

Jacques-Coper M, Brönnimann S. 2014. Summer temperature in the eastern part of southern South America: its variability in the twentieth century and a teleconnection with oceania. *Clim. Dyn.*, doi: 10.1007/s00382-013-2038-8.

Kalnay E, Kanamitsu M, Kistler R, Collins W, Deaven D, Gandin L, Iredell M, Saha S, White G, Woollen J, Zhu Y, Leetmaa A, Reynolds R, Chelliah M, Ebisuzaki W, Higgins W, Janowiak J, Mo KC, Ropelewski C, Wang J, Jenne R, Joseph D. 1996. The NCEP/NCAR 40-year reanalysis project. *Bull. Am. Meteorol. Soc.* **77**: 437–471, doi: 10.1175/1520-0477(1996)077<0437:TNYRP>2.0.CO;2.

Kayano MT, de Oliveira CP, Andreoli RV. 2009. Interannual relations between South American rainfall and tropical sea surface temperature anomalies before and after 1976. *Int. J. Climatol.* **29**: 1439–1448, doi: 10.1002/joc.1824.

Kerr RA. 1992. Unmasking a shifty climate system. *Science* **255**: 1508–1510, doi: 10.1126/science.255.5051.1508.

Legates DR, Willmott CJ. 1990a. Mean seasonal and spatial variability in gauge-corrected, global precipitation. *Int. J. Climatol.* **10**: 111–127, doi: 10.1002/joc.3370100202.

Legates DR, Willmott CJ. 1990b. Mean seasonal and spatial variability in global surface air temperature. *Theor. Appl. Climatol.* **41**: 11–21, doi: 10.1007/BF00866198.

Liebmann B, Vera CS, Carvalho LMV, Camilloni IA, Hoerling MP, Allured D, Barros VR, Báez J, Bidegain M. 2004. An observed trend in central South American precipitation. *J. Clim.* **17**: 4357–4367, doi: 10.1175/3205.1.

Litzow MA. 2006. Climate regime shifts and community reorganization in the Gulf of Alaska: how do recent shifts compare with 1976/1977? *ICES J. Mar. Sci.* **63**: 1386–1396, doi: 10.1016/j.icesjms.2006.06.003.

Mantua N, Hare S. 2002. The Pacific Decadal Oscillation. *J. Oceanogr.* **58**: 35–44, doi: 10.1023/A:1015820616384.

Mantua NJ, Hare SR, Zhang Y, Wallace JM, Francis RC. 1997. A pacific interdecadal climate oscillation with impacts on salmon production. *Bull. Am. Meteorol. Soc.* **78**: 1069–1079, doi: 10.1175/1520-0477(1997)078<1069:APICOW>2.0.CO;2.

Marengo JA. 2004. Interdecadal variability and trends of rainfall across the Amazon basin. *Theor. Appl. Climatol.* **78**: 79–96, doi: 10.1007/s00704-004-0045-8.

Meehl GA, Hu A, Santer BD. 2009. The mid-1970s climate shift in the pacific and the relative roles of forced versus inherent decadal variability. *J. Clim.* **22**: 780–792, doi: 10.1175/2008JCLI2552.1.

Miller AJ, Cayan DR, Barnett TP, Graham NE, Oberhuber JM. 1994. The 1976–77 climate shift of the Pacific Ocean. *Oceanography* **7**: 21–26, doi: 10.5670/oceanog.1994.11.

Minobe S. 1997. A 50–70 year climatic oscillation over the North Pacific and North America. *Geophys. Res. Lett.* **24**: 683–686, doi: 10.1029/97GL00504.

Montecinos A, Purca S, Pizarro O. 2003. Interannual-to-interdecadal sea surface temperature variability along the western coast of South America. *Geophys. Res. Lett.* **30**: 1570, doi: 10.1029/2003GL017345.

Montecinos A, Leth O, Pizarro O. 2007. Wind-driven interdecadal variability in the eastern tropical and South Pacific. *J. Geophys. Res.* **112**: 1–8, doi: 10.1029/2006JC003571.

Narayan N, Paul A, Mulitza S, Schulz M. 2010. Trends in coastal upwelling intensity during the late 20th century. *Ocean Sci.* **6**: 815–823, doi: 10.5194/os-6-815-2010.

Peterson TC, Vose RS. 1997. An overview of the Global Historical Climatology Network Temperature Database. *Bull. Am. Meteorol. Soc.* **78**: 2837–2849, doi: 10.1175/1520-0477(1997)078<2837:AOOTGH>2.0.CO;2.

Piovano EL, Ariztegui D, Moreira SD. 2002. Recent environmental changes in Laguna Mar Chiquita (central Argentina): a sedimentary model for a highly variable saline lake. *Sedimentology* **49**: 1371–1384, doi: 10.1046/j.1365-3091.2002.00503.x.

Pizarro O, Montecinos A. 2004. Interdecadal variability of the thermocline along the west coast of South America. *Geophys. Res. Lett.* **31**: L20307, doi: 10.1029/2004GL020998.

Pizarro O, Hormazabal S, Gonzalez A, Yañez E. 1994. Variabilidad del viento, nivel del mar y temperatura en la costa norte de Chile. *Investig. Mar.* **22**: 85–101.

Power S, Casey T, Folland C, Colman A, Mehta V. 1999. Inter-decadal modulation of the impact of ENSO on Australia. *Clim. Dyn.* **15**: 319–324, doi: 10.1007/s003820050284.

Quintana JM, Aceituno P. 2012. Changes in the rainfall regime along the extratropical west coast of South America (Chile): 30-43°S. *Atmósfera* **25**: 1–22. http://www.revistas.unam.mx/index.php/atm/article/view/29080 (accessed 19 July 2012).

Rayner NA, Parker DE, Horton EB, Folland CK, Alexander LV, Rowell DP, Kent EC, Kaplan A. 2003. Global analyses of sea surface temperature, sea ice, and night marine air temperature since the late nineteenth century. *J. Geophys. Res. Atmos.* **108**: 4407, doi: 10.1029/2002JD002670.

Rodionov SN. 2005. A sequential method for detecting regime shifts in the mean and variance. In *Large-Scale Disturbances (Regime Shifts) and Recovery in Aquatic Ecosystems: Challenges for Management Toward Sustainability*, Velikova V, Chipev N (eds). UNESCO-ROSTE/BAS Workshop on Regime Shifts, 14–16 June 2005, Varna, Bulgaria, 68–72.

Schulz N, Boisier JP, Aceituno P. 2012. Climate change along the arid coast of northern Chile. *Int. J. Climatol.* **32**: 1803–1814, doi: 10.1002/joc.2395.

Smith TM, Reynolds RW, Peterson TC, Lawrimore J. 2008. Improvements to NOAA's historical merged land–ocean surface temperature analysis (1880–2006). *J. Clim.* **21**: 2283–2296, doi: 10.1175/2007JCLI2100.1.

Tanimoto Y, Hanawa K, Toba Y, Iwasaka N. 1993. Characteristic variations of sea surface temperature with multiple time scales in the North Pacific. *J. Clim.* **6**: 1153–1160, doi: 10.1175/1520-0442(1993)006<1153:CVOSST>2.0.CO;2.

Trenberth KE. 1990. Recent observed interdecadal climate changes in the Northern Hemisphere. *Bull. Am. Meteorol. Soc.* **71**: 988–993, doi: 10.1175/1520-0477(1990)071<0988:ROICCI>2.0.CO;2.

Uppala SM, Kållberg PW, Simmons AJ, Andrae U, Bechtold VDC, Fiorino M, Gibson JK, Haseler J, Hernandez A, Kelly GA, Li X, Onogi K, Saarinen S, Sokka N, Allan RP, Andersson E, Arpe K, Balmaseda MA, Beljaars ACM, Berg L Van De, Bidlot J, Bormann N, Caires S, Chevallier F, Dethof A, Dragosavac M, Fisher M, Fuentes M, Hagemann S, Hólm E, Hoskins BJ, Isaksen L, Janssen PAEM, Jenne R, Mcnally AP, Mahfouf J-F, Morcrette J-J, Rayner NA, Saunders RW, Simon P, Sterl A, Trenberth KE, Untch A, Vasiljevic D, Viterbo P, Woollen J. 2005. The ERA-40 re-analysis. *Q. J. R. Meteorol. Soc.* **131**: 2961–3012, doi: 10.1256/qj.04.176.

Vargas G, Pantoja S, Rutllant JA, Lange CB, Ortlieb L. 2007. Enhancement of coastal upwelling and interdecadal ENSO-like variability in the Peru-Chile current since late 19th century. *Geophys. Res. Lett.* **34**: L13607, doi: 10.1029/2006GL028812.

Yasunaka S, Hanawa K. 2005. Regime shift in the global sea-surface temperatures: its relation to El Niño–southern oscillation events and dominant variation modes. *Int. J. Climatol.* **25**: 913–930, doi: 10.1002/joc.1172.

Zhang Y, Wallace JM, Battisti DS. 1997. ENSO-like Interdecadal Variability: 1900–93. *J. Clim.* **10**: 1004–1020, doi: 10.1175/1520-0442(1997)010<1004:ELIV>2.0.CO;2.

Zhang R-H, Rothstein LM, Busalacchi AJ. 1998. Origin of upper-ocean warming and El Nino change on decadal scales in the tropical Pacific Ocean. *Nature* **391**: 879–883, doi: 10.1038/36081.

